International Journal of Fatigue 96 (2017) 208–223

Contents lists available at ScienceDirect

International Journal of Fatigue

journal homepage: www.elsevier.com/locate/ijfatigue

Fatigue life calculation for a specimen with an impact pit considering impact damage, residual stress relaxation and elastic-plastic fatigue damage

Zhan Zhixin [a], Hu Weiping [a,*], Shen Fei [b], Meng Qingchun [a], Pu Jing [a], Guan Zhidong [a]

[a] School of Aeronautics Science and Engineering, Beihang University, Beijing 100191, China
[b] School of Mechanical and Aerospace Engineering, Nanyang Technological University, Singapore 639798, Singapore

ARTICLE INFO

Article history:
Received 25 August 2016
Received in revised form 28 November 2016
Accepted 29 November 2016
Available online 1 December 2016

Keywords:
Damage mechanics
Fatigue life
Impact damage
Residual stress
Elastic-plastic

ABSTRACT

In this study, a continuum damage mechanics based method is proposed to calculate the fatigue life of a specimen with an impact pit. The impact process is simulated by a quasi-static analysis. The residual stress and the impact damage are calculated. Then, the elastic-plastic fatigue damage of the material is considered as the specimen experiences cyclic loading. The residual stress relaxation is investigated via a coupled analysis of the residual stress and elastic-plastic damage evolution. The calculated results agree well with the experimental results. The effects of the impact depth and radius that the impact object has on the fatigue failure are also discussed.

1. Introduction

In the process of manufacturing, assembling or servicing engineering structures, defects, such as impact pits, tend to be generated on the surfaces of structures due to an accidental bump or a drop of a foreign object [1,2]. An impact pit has a non-negligible negative effect on the fatigue life of structures. However, if all structures containing impact damage are considered unfit for service, a great deal of waste will be generated, as some damaged structures are still able to sustain cyclic loading and even meet the fatigue life requirements [3]. A reasonable and effective method is necessary to quantitatively evaluate the influence caused by impact damage and to accurately predict the fatigue life of a structure containing an impact defect.

Fatigue life prediction of components is an important issue in engineering applications. Some methods have been proposed and practically used. The local stress strain method [4], based on the stress-strain course at the notch root in combination with the material fatigue characteristic curve, is convenient to use. However, this method is confined to some simple cases. The critical plane method [5] has been applied more widely due to its board applicability and good accuracy by presenting a semi-empirical formulation expressed with the maximum fatigue damage parameter over a number of different planes. However, the parameter lacks explicit physical significance. These several methods utilized for plain fatigue problems cannot be directly used for failure analyses of structures with impact damage due to the complex effects induced by the impact. The impact damage [6–8] can influence the subsequent fatigue life of components by three main factors: (i) impact-induced residual stresses, (ii) impact damage associated with local plastic deformation, and (iii) local stress concentrations around the impact pit. The continuum damage mechanics based method [9–11], which is a relatively new method developed in recent decades, also has the capability of analyzing fatigue failure in structures. This method describes the damage evolution process using damage variables and has been widely used to address a number of practical problems. Better yet, the continuum damage mechanics method can reasonably analyze the three effects induced by impact damage and present quantitative results and the process of damage evolution.

In the previous work [12], fatigue life calculations for defected structure were conducted, which considered the effects of the initial impact damage associated with the local plastic deformation and the local stress concentrations around the impact pit. However, the initial residual stress was assumed to remain unchanged and its effect was measured by simply superposing the cyclic stress due to the total stress on the specimen being less than the yield

* Corresponding author at: Room D604, New Main Building, 37th Xueyuan Road, Beihang University, Beijing 100191, China.
E-mail address: huweiping@buaa.edu.cn (W. Hu).

http://dx.doi.org/10.1016/j.ijfatigue.2016.11.036
0142-1123/

stress. Thus, the residual stress relaxation and plastic damage were not taken into account. In the material around the impact pit, it is easy to incur plastic deformation because of the effect of the stress concentration as cyclic loading increases. Therefore, on one hand, it is necessary to consider the elastic-plastic fatigue damage in the fatigue life calculation. Meanwhile, the residual stress field will vary when the specimen experiences inelastic deformation. Thus, the effect of residual stress relaxation also needs to be considered. The effect of residual stresses on the fatigue life of structures has been extensively studied for years and is reasonably well understood [13–15]. In particular, near surface tensile residual stresses tend to accelerate the initiation and growth phases of the fatigue process, whereas compressive residual stresses close to a surface may prolong the fatigue life. However, the residual stress state induced by the impact of a projectile onto a metallic surface can be significantly altered during subsequent fatigue loading. Studies [16–22] have shown that the relaxation of residual stress occurs during cyclic loading and the rate of residual stress relaxation can be significant in the early stages of cyclic loading. In some cases, residual stress can be entirely relaxed in the first few load cycles. Such mechanical cycle-dependent redistribution of residual stresses is often termed cyclic relaxation [23,24]. Therefore, it is difficult to accurately predict the residual stress relaxation effect. Through experiments, Mattson and Coleman [25] observed cyclic residual stress relaxation many years ago and found that their predicted fatigue lives were shorter than the experimental results if residual stress relaxation was not taken into consideration. A theoretical method to describe this phenomenon is still required.

This study examines the issues of elastic-plastic fatigue damage and the corresponding effect that it has on residual stress relaxation. Specimens fabricated from TC4 are investigated in this work. The calculated results based on the proposed model are validated by the experimental results obtained by Peters [8]. First, to address the impact damage, impact-induced residual stress, and interactions between inelastic fatigue damage and residual stress relation, a quasi-static numerical simulation of the impact process is conducted. From this, the initial residual stress field and plastic strain field around the impact pit is obtained. Then, the initial impact damage can be calculated according to Lemaitre's ductile damage model. Second, the damage coupled elastic-plastic constitutive equations are adopted as the material model, and the inelastic damage evolution equations are used to evaluate the extent of the damage of material after a certain number of loading cycles. By virtue of the FE implementation used in ABAQUS, the effects of impact damage and residual stress are considered, and the interactions between inelastic damage evolution and residual stress relaxation are presented as well. The calculated fatigue life and residual stress relaxation effect are found to be in accordance with the experimental results. Additionally, some factors influencing elastic-plastic damage and fatigue life are also discussed.

2. Theoretical models

2.1. Impact stress analysis and initial impact damage analysis model

2.1.1. Initial stress analysis

In this study, a quasi-static numerical method is applied to simulate the foreign object impact process. This is based on two aspects. On one hand, the dynamic simulation of the impact process is time-consuming and the computational results are sometimes instable. On the other hand, it is easier to continually implement subsequent fatigue damage analysis using a quasi-static simulation than follow a dynamic simulation. To obtain equivalent results between the quasi-static simulations and dynamic simulations, the energy equivalence method [26] and experimental measurements of dynamic impact [27] need to be adopted, which guarantee that the static indentation and initial residual stress state of the quasi-static analysis are equivalent to the dynamic impact damage [23].

In the quasi-static simulation, considering the stiffness of the foreign object is much higher than that of the structure material, it is reasonable to regard the foreign object as a rigid body and the structure as an elastoplastic body. The elastic-plastic constitutive model proposed by Lemaitre and Chaboche [28] is used to describe the constitutive relationship of the structure material. During impact, large strains first form at the contact surface, and then, the strain diffuses in the vicinity of the contact surface. Once the impact process is completed, residual stresses and plastic strains exist in the zone around the impact pit.

2.1.2. Initial impact damage analysis model

Deterioration of material induced by an impact can be represented by the damage variable in the framework of continuum damage mechanics. Lemaitre and Chaboche [29] have presented the fundamental concepts of continuum damage mechanics. For the case of isotropic damage of isotropic materials, the damage variable D can be represented by the deterioration ratio of the stiffness of RVE (Representative Volume Element), which is expressed by:

$$D = \frac{E - E_D}{E}, \tag{1}$$

where E is the Young's Modulus of the material and E_D is the effective Young's Modulus of the RVE with damage. The value of E_D ranges from E to 0, and the value of D varies between 0 and 1.

After completion of the residual stress analysis, the initial damage induced by plastic deformation can be calculated according to Lemaitre's ductile damage model [30]:

$$\dot{D} = \left(\frac{\sigma_{eq}^2 R_v}{2ES(1-D)^2}\right)^s \dot{p}, \tag{2}$$

where σ_{eq} is the equivalent stress, $\dot{p}$ is the rate of accumulated plastic strain, S and s are material parameters, R_v is the triaxiality function: $R_v = \frac{2}{3}(1+\mu) + 3(1-2\mu)\left(\frac{\sigma_H}{\sigma_{eq}}\right)^2$, and σ_H is the hydrostatic stress.

This formula can be integrated over time to calculate the initial damage induced by the impact as follows:

$$D_0 = \left(\frac{\sigma_{eq\max}^2 R_v}{2ES}\right)^s \Delta p, \tag{3}$$

where Δp is the accumulated plastic strain over this period.

2.2. Fatigue damage analysis model

2.2.1. Damage-coupled elastic-plastic constitutive model

In the framework of a small deformation, the total strain ε_{ij} can be decomposed into:

$$\varepsilon_{ij} = \varepsilon_{ij}^e + \varepsilon_{ij}^p, \tag{4}$$

where ε_{ij}^e and ε_{ij}^p are the elastic and plastic strains, respectively. In the damage-coupled constitutive model, the damage is coupled with elasticity or plasticity using the effective stress instead of the stress in the elasticity law and the von Mises yield criterion. Based on the hypothesis of strain equivalence, the elastic strain takes the form of:

$$\varepsilon_{ij}^e = \frac{1+\upsilon}{E}\left(\frac{\sigma_{ij}}{1-D}\right) - \frac{\upsilon}{E}\left(\frac{\sigma_{kk}\delta_{ij}}{1-D}\right), \tag{5}$$

where E, v and σ_{ij} are the Young's Modulus, Poisson's ratio and stress components, respectively, and δ_{ij} is the Kronecker delta: $\delta_{ij} = \begin{cases} 0, & if\ i \neq j \\ 1, & if\ i = j \end{cases}$. The subscripts i and j have values of 1, 2, or 3. The evolution of plastic strain is defined as:

$$\dot{\varepsilon}^p = \dot{\lambda}\frac{\partial f}{\partial \sigma_{ij}}, \tag{6}$$

where $\dot{\lambda}$ is the plastic multiplier. The nonlinear kinematic hardening model proposed by Chaboche [31] is used to represent the kinematic hardening behavior. The von Mises yield function f with damage is expressed as:

$$f = \sqrt{\frac{3}{2}\left(\frac{S_{ij}}{1-D} - \alpha_{ij}\right)\left(\frac{S_{ij}}{1-D} - \alpha_{ij}\right)} - Q, \quad \text{where} \quad \alpha_{ij} = \sum_{k=1}^{M}\alpha_{ij}^{(k)}, \tag{7}$$

S_{ij} is the deviatoric part of the stress, α_{ij} is the deviatoric part of the back stress, and Q is the radius of the yield surface, and its evolution is defined as:

$$\dot{Q} = \dot{\lambda}b(Q_\infty - Q), \tag{8}$$

where the parameters b and Q_∞ are material constants. The variable $\dot{\lambda}$ can be determined by the plastic flow consistency condition: $f = \dot{f} = 0$. The evolution of plastic strain components [28] can be obtained as:

$$\dot{\varepsilon}^p = \frac{3}{2}\frac{\dot{\lambda}}{1-D}\frac{S_{ij}/(1-D) - \alpha_{ij}}{(S_{ij}/(1-D) - \alpha_{ij})_{eq}}, \tag{9}$$

$$\dot{p} = \sqrt{\frac{2}{3}\dot{\varepsilon}_{ij}^p\dot{\varepsilon}_{ij}^p} = \frac{\dot{\lambda}}{1-D}, \tag{10}$$

$$\dot{\alpha}_{ij}^{(k)} = (1-D)\left(\frac{2}{3}C_k\dot{\varepsilon}_{ij}^p - \gamma_k\alpha_{ij}^{(k)}\dot{p}\right), \tag{11}$$

where $\dot{p}$ is the accumulated plastic strain rate and C_k and γ_k are material constants determined from experimental tests.

2.2.2. Fatigue damage evolution model

After the impact is completed, fatigue loading is applied. In view of the fact that the superposition of the applied cyclic stress and residual stress may be greater than the yield stress, the elastic and inelastic damage evolution models both need to be employed to calculate the extent of damage of the material. According to the analysis performed by Kang [32], total damage of the material can be decomposed into two parts: elastic damage and plastic damage. The elastic damage is dependent on the state of cyclic stress, and the plastic damage is governed by the accumulated plastic strain over each fatigue cycle. The expression is:

$$D = D_e + D_p. \tag{12}$$

For multi-axial cyclic loading, the elastic damage evolution equation [33,34] for the non-linear continuous damage model can be written as:

$$\dot{D}_e = \frac{dD_e}{dN} = \left[1 - (1-D)^{\beta+1}\right]^{\alpha} \cdot \left[\frac{A_{II}}{M_0(1 - 3b_2\sigma_{H,m})(1-D)}\right]^{\beta}, \tag{13}$$

where N is the number of cycles until failure; α, β, M_0 and b_2 are material constants determined by fatigue tests; and A_{II} is the amplitude of the octahedral shear stress, which is defined by:

$$A_{II} = \frac{1}{2}\left[\frac{3}{2}\left(S_{ij,\max} - S_{ij,\min}\right)\cdot\left(S_{ij,\max} - S_{ij,\min}\right)\right]^{1/2}, \tag{14}$$

where $S_{ij,\max}$ and $S_{ij,\min}$ are the maximum and the minimum values of the deviatoric stress tensor ij components during one loading cycle. The variable $\sigma_{H,m}$ is the mean hydrostatic stress and is defined by:

$$\sigma_{H,m} = \frac{1}{6}[\max(tr(\sigma)) + \min(tr(\sigma))], \tag{15}$$

where $tr(\sigma) = \sigma_{11} + \sigma_{22} + \sigma_{33}$.

Table 1
Chemical composition of the TC4 titanium alloy (in weight percent).

Al	Fe	V	C	N	H	O	Ti
5.50	0.30	3.50	0.10	0.05	0.02	0.15	90.38

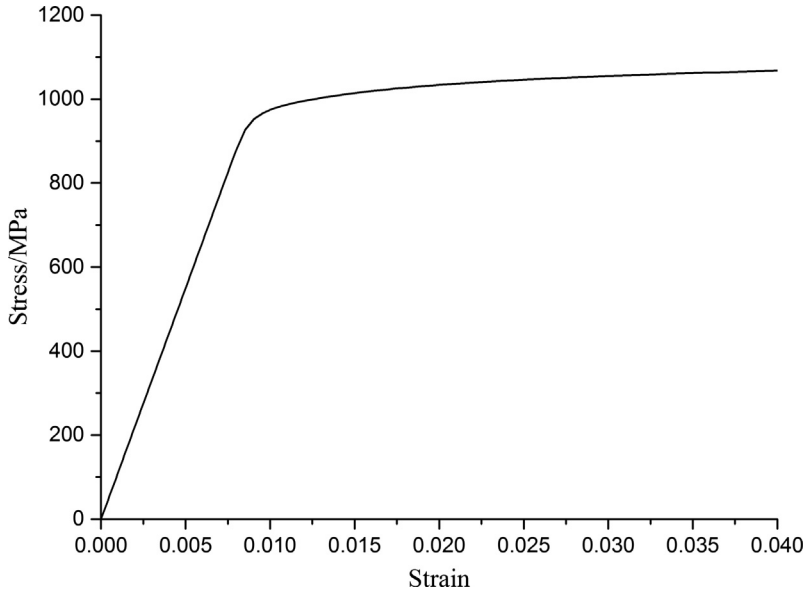

Fig. 1. Stress-strain curve for the TC4 titanium alloy.

Table 2
Static mechanical and material parameters for the TC4 titanium alloy.

E/MPa	ν	σ_y/MPa	C_1/MPa	C_2/MPa	C_3/MPa	γ_1	γ_2	γ_3
110,000	0.33	940	110,840	10,891	1829	1446	163	18

The parameter α is defined by:

$$\alpha = 1 - a\left\langle \frac{A_{II} - A_{II}^*}{\sigma_u - \sigma_{e,\max}} \right\rangle, \tag{16}$$

where $\sigma_{e,\max}$ is the maximum equivalent stress over a loading cycle. The Sines fatigue limit criterion A_{II}^* in this model is determined from:

$$A_{II}^* = \sigma_{l0}(1 - 3b_1\sigma_{H,m}). \tag{17}$$

By integrating Eq. (13) from $D = 0$ to $D = 1$ for the case of a cyclic stress with a constant amplitude, the number of cycles to failure N_F is obtained as:

$$N_F = \frac{1}{1+\beta} \cdot \frac{1}{aM_0^{-\beta}} \frac{\langle \sigma_u - \sigma_{e,\max} \rangle}{\langle A_{II} - A_{II}^* \rangle} \cdot \left(\frac{A_{II}}{1 - b_2\sigma_{H,m}} \right)^{-\beta}. \tag{18}$$

The plastic damage evolution equation can be written as:

$$\dot{D}_p = \left(\frac{\sigma_{eq}^2 R_v}{2ES(1-D)^2} \right)^s \dot{p}. \tag{19}$$

The variables in Eq. (19) are explained in Section 2.1.2.

3. Material parameters calibration for TC4

The material TC4 titanium alloy is studied in this paper. The chemical composition of this material is presented in Table 1. Three types of material parameters need to be calibrated: (i) material parameters for the elastic–plastic constitutive model, (ii) material parameters for the elastic damage evolution model, and (iii) material parameters for the plastic damage evolution model.

3.1. Calibration of parameters in the elastic-plastic constitutive model

The stress-strain curve obtained from the uniaxial tensile test shown in Fig. 1 is used to determine the parameters in the constitutive equations. In this study, the isotropic hardening is neglected and three components of back stress are adopted to represent the nonlinear kinematic hardening behavior, which can be expressed as an exponential saturation equation:

$$\sigma = \sigma_y + \sum_{k=1}^{n} \frac{C_k}{\gamma_k}(1 - e^{-\gamma_k \varepsilon_p}), \tag{20}$$

Table 3
Material parameters in the elastic damage model for TC4 titanium alloy.

β	M_0	b_1	b_2	a
1.95	114,339	0.0015	0.00045	0.72

Table 4
Material parameters in the plastic damage evolution model for TC4 titanium alloy.

S/MPa	m
14,429	0.2976

where σ_y and ε_p are the initial yield stress and the plastic strain, respectively. The least squares method is adopted to calibrate parameters. The result of the calibration is presented in Table 2.

3.2. Calibration of parameters in the elastic damage evolution model

There are five parameters, β, a, M_0, b_1 and b_2, in the elastic damage evolution equation. First, four material parameters, β, $1/((1+\beta)aM_0^{-\beta})$, b_1 and b_2, are determined from the fatigue experimental data for smooth specimens. In the case of smooth specimens subjected to uniaxial fatigue loading, a closed form expression of fatigue life can be derived, which is similar to that

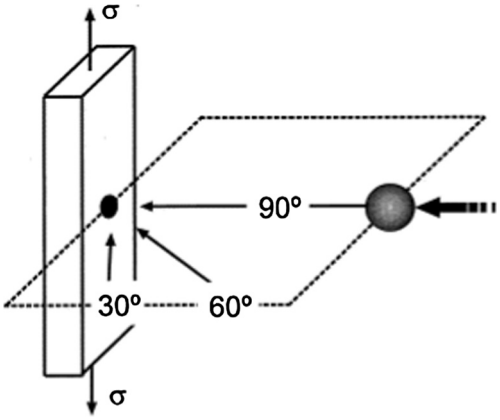

Fig. 2. A schematic illustration of the impact angle [8].

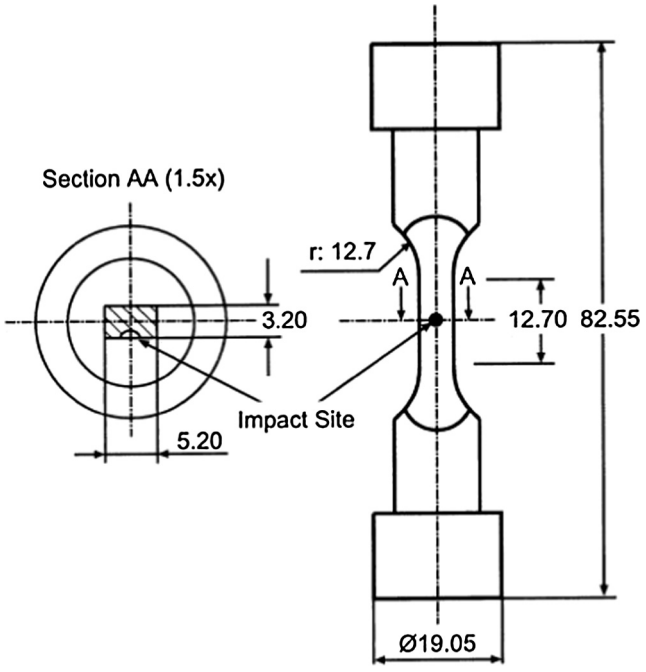

Fig. 3. The geometry of the specimen (all dimensions are in mm) [8].

in Eq. (18). Therefore, parameters β and $1/((1+\beta)aM_0^{-\beta})$ are readily identified from the fatigue test data for a stress ratio of $R = -1$. Then, using the least squares method, parameters b_1 and b_2 are obtained from the fatigue tests data at other stress ratios.

Finally, the independent parameters a and M_0 are identified numerically using the damage mechanics–finite element method [35–37]. The fatigue test data for the TC4 titanium alloy is taken from the literature [38]. The calibrated parameters for the elastic damage evolution model are listed in Table 3.

3.3. Calibration of the parameters in the plastic damage evolution model

There are two parameters, m and S, in the plastic damage evolution model, which can be calibrated from strain-controlled low-cycle fatigue test data. For the uniaxial case, the number of cycles to failure can be obtained by integrating Eq. (19) from $D = 0$ to $D = 1$:

Table 5
The fatigue experiment results [8] and calculated results.

The depth of impact/mm	σ_{max}/MPa	$\Delta\sigma$/MPa	Experiment results/Cycle	Calculated results/Cycle
0.43	500	450	75,000	133,150
0.43	500	450	140,000	
0.54	500	450	80,000	76,250
0.54	500	450	78,000	
0.54	500	450	82,000	
0.67	500	450	46,000	62,050
0.67	500	450	34,000	
0.67	500	450	65,000	

$$N_f = \frac{1}{2(2m+1)\Delta\varepsilon_p}\left(\frac{2ES}{(\sigma_{max})^2}\right)^m, \tag{21}$$

using the cyclic stress–strain curve described as:

$$\sigma_{max} = K'\left(\frac{\Delta\varepsilon_p}{2}\right)^{n'}, \tag{22}$$

where K' and n' are parameters obtained from experiments. Then, Eq. (21) can be expressed as:

$$N_f = \frac{1}{2(2m+1)}\left(\frac{2^{1+2n'}ES}{(K')^2}\right)(\Delta\varepsilon_p)^{-(1+2mn')}. \tag{23}$$

The values of ε_f', c, K' and n' are obtained from low-cycle fatigue tests data [39].

According to the Coffin-Manson law, the strain-life curve can be expressed as:

$$\frac{\Delta\varepsilon_p}{2} = \varepsilon_f'(2N_f)^c, \tag{24}$$

where ε_f' and c are material parameters.

Comparing Eq. (23) with Eq. (24), the parameters in the plastic damage evolution model can be determined, as listed in Table 4.

4. Experiments and numerical simulation

4.1. Experiments

The foreign object impact experiments and subsequent fatigue experiments on TC4 specimens were performed by Peters [8]. A brief overview of the experiments is presented here.

Foreign object impact damage was introduced by firing 3.2 mm diameter chrome-hardened steel spheres onto the surfaces of flat

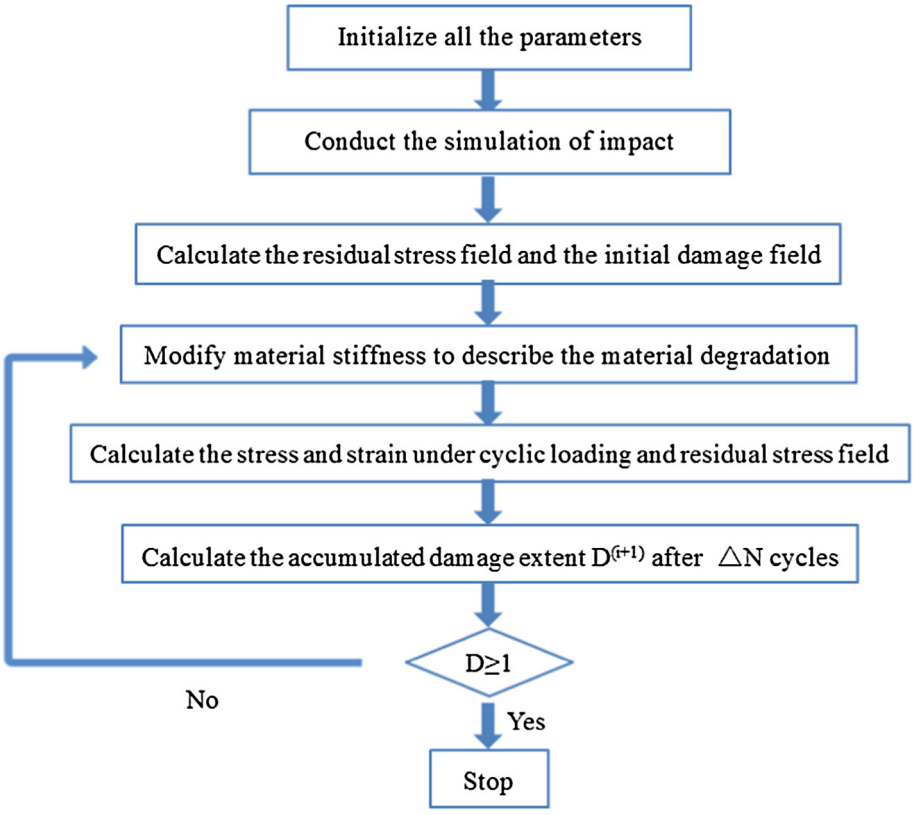

Fig. 4. The flowchart for the FE computational methodology.

tensile fatigue specimens at an angel of 90° (normal impact) at velocities of 200, 250 and 300 m/s using a compressed-gas gun facility. These velocities represent typical in-service impact velocities on aircraft engine fan blades. After the impact was completed, the impact depth was measured, with the corresponding impact depths of 0.43 mm, 0.54 mm and 0.67 mm. A schematic illustration of the impact angle is shown in Fig. 2 [8], and the geometry of the specimen is shown in Fig. 3.

After impact, the specimens were subsequently loaded on an automated MTS servo-hydraulic testing machine using a loading of the frequency of 20 Hz and a stress ratio of $R = 0.1$ with a nominal maximum stress of 500 MPa. The experimental results are shown in Table 5.

4.2. Computational methodology

The entire numerical computation of the fatigue life of a specimen with an impact pit includes simulation of the impact process, calculation of the residual stress, computation of the initial impact damage, and calculation of the elastic-plastic fatigue damage. The

Table 6
The maximum values of longitudinal residual stress from impact simulation corresponding to the different mesh sizes.

	Mesh size 1#	Mesh size 2#	Mesh size 3#
Minimum element size	0.095 mm × 0.095 mm × 0.132 mm	0.086 mm × 0.086 mm × 0.106 mm	0.075 mm × 0.075 mm × 0.095 mm
Stress/MPa	510.6	515.2	518.1
Relative Error	0.90%	0.56%	

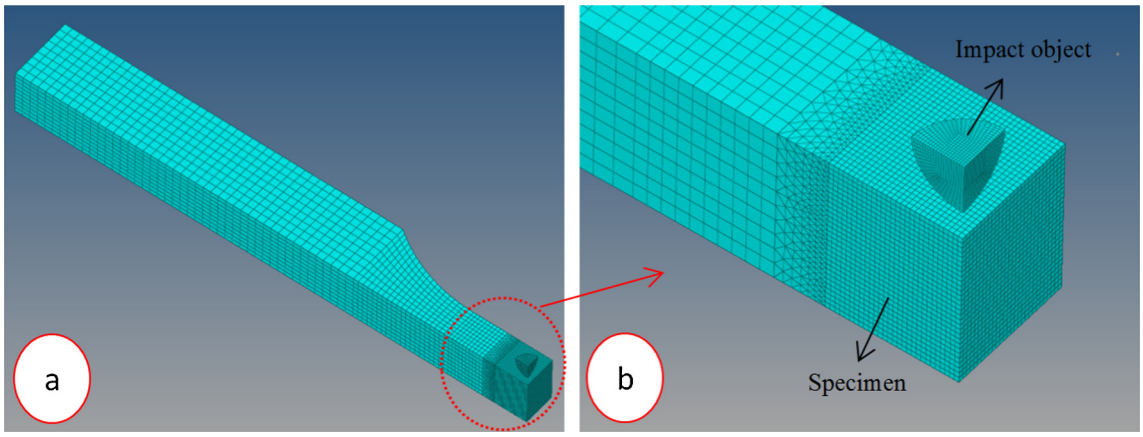

Fig. 5. The established finite element model: (a) the global view and (b) the local view.

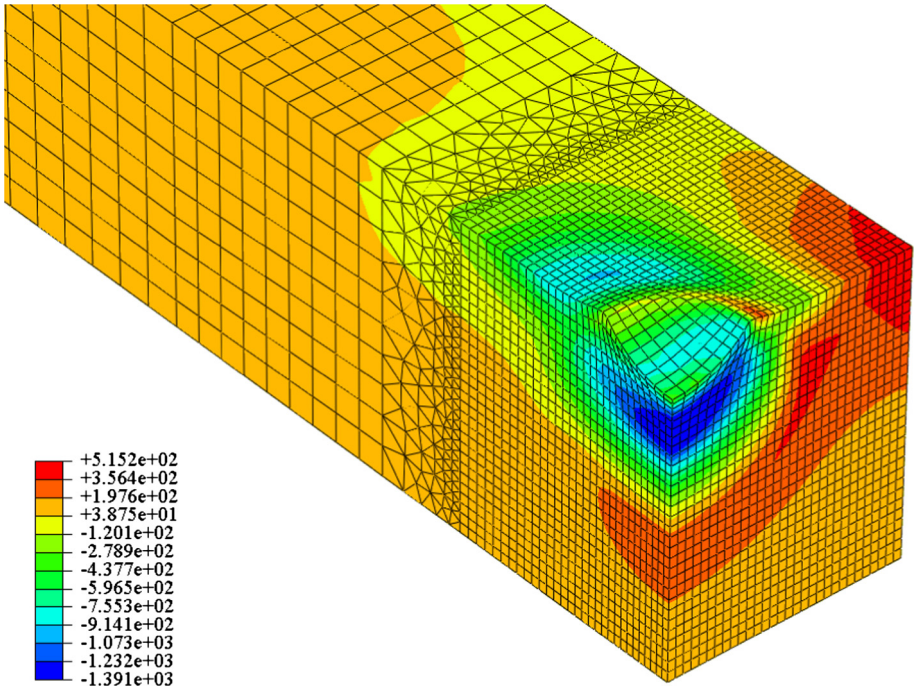

Fig. 6. The distribution of the longitudinal residual stress around the impact pit (MPa).

user subroutines UMAT in ABAQUS are used to implement the damage-coupled elastic–plastic constitutive model and fatigue damage evolution models.

As the flowchart in Fig. 4 illustrates, the detailed steps of the calculation are:

(1) Initialize all of the parameters and set the initial value of the damage extent D to zero.
(2) Conduct a quasi-static simulation analysis of the impact process to obtain the plastic strain and residual stress fields.
(3) Calculate the initial damage field associated with the plastic deformation during the impact process using Lemaitre's ductile damage model.
(4) Modify the material properties for each element according to the initial damage extent D_0. Then, calculate the cyclic stress and accumulated plastic strain for one loading cycle using ABAQUS considering the residual stress field induced by the impact.
(5) Since it is very time-consuming to calculate the fatigue damage cycle by cycle, the jump-in-cycle procedure is adopted in the numerical implementation, which assumes that the cyclic stresses and damage remain unchanged for each cycle during a block of ΔN cycles. The increment of fatigue damage is calculated based on Eqs. (13) and (19) after experiencing ΔN cycles, which is given as:

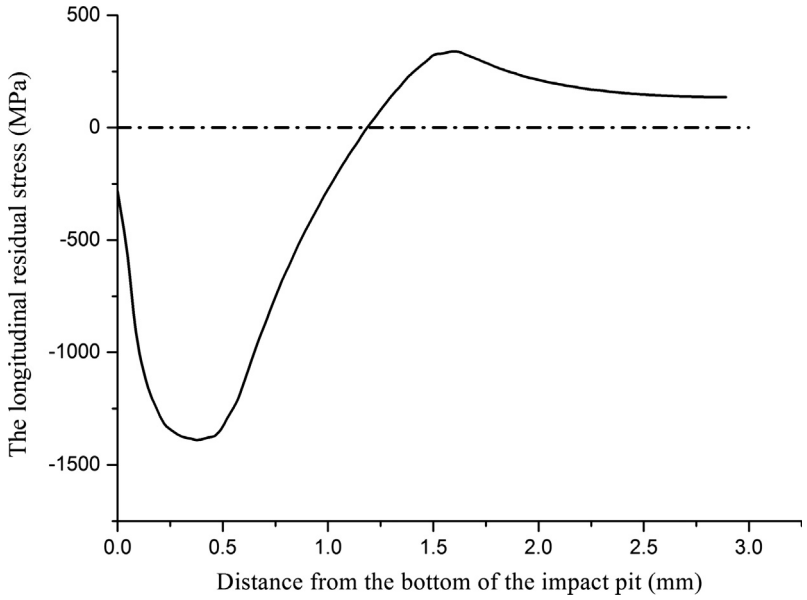

Fig. 7. The distribution of the longitudinal residual stress along the distance from the bottom of the impact pit.

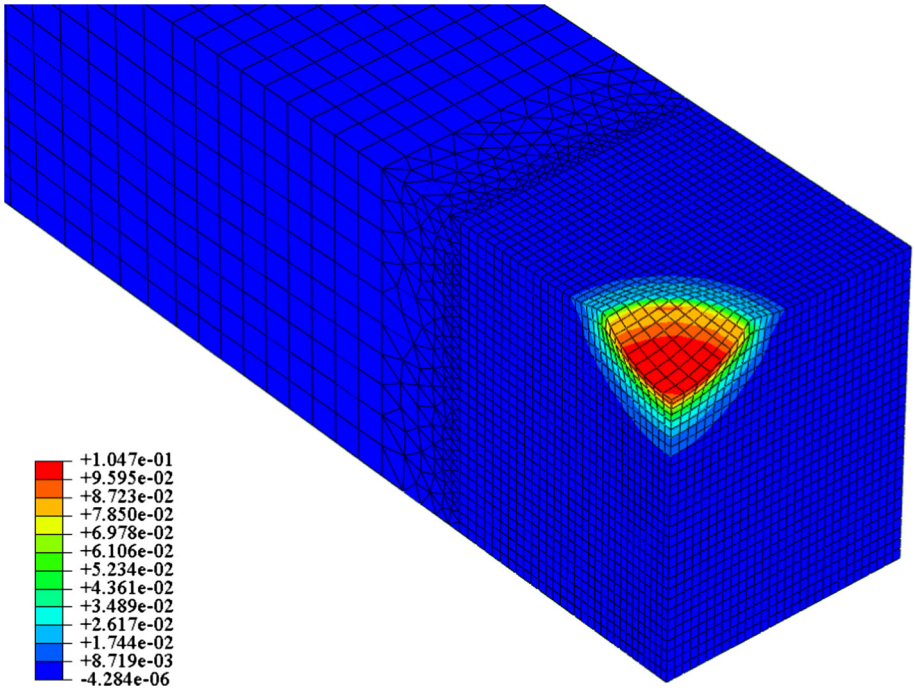

Fig. 8. The distribution of the initial impact damage field around the impact pit.

$$\Delta D^{(i+1)} = \begin{cases} \Delta N \cdot \dot{D}_e^{(i+1)}, \text{only elastic damage occurs} \\ \dot{D}_e^{(i+1)} + \dot{D}_p^{(i+1)}, \text{elastic} - \text{plastic damage occurs} \end{cases}. \quad (25)$$

Then, the total extent of damage corresponding to the number of cycles N is obtained as:

$$D^{(i+1)} = D^{(i)} + \Delta D^{(i+1)}. \quad (26)$$

(6) If the accumulation of damage at any element reaches 1, a fatigue crack is assumed to initiate at this element and the corresponding number of cycles is the fatigue crack initiation life. Otherwise, a recalculation of the material properties of each element is conducted using the equation:

$$E^{(i+1)} = E^{(i)}(1 - D^{(i+1)}). \quad (27)$$

Then, analyses of the stress field and the damage field are repeated until the accumulation of damage at any element reaches 1.

4.3. Numerical simulation

4.3.1. Quasi-static simulation analysis of the impact process

In this section, the finite element analysis software ABAQUS is used to simulate the impact process in a quasi-static way. The geometry of specimen for the simulated foreign object damage studies is shown in Fig. 3. A quarter symmetry model is built and symmetry boundary conditions are applied at the plane of symmetry. The foreign object is set as rigid, and the structure is set as elastoplastic. A 3-D 8-node solid element is used, which is defined by eight nodes, with three degrees of freedom per node. The

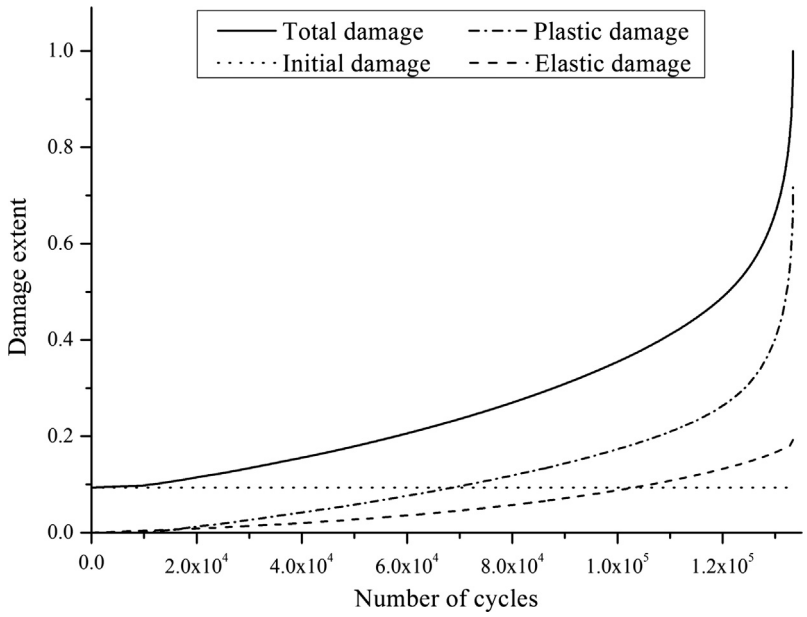

Fig. 9. Extent of the damage versus the number of cycles.

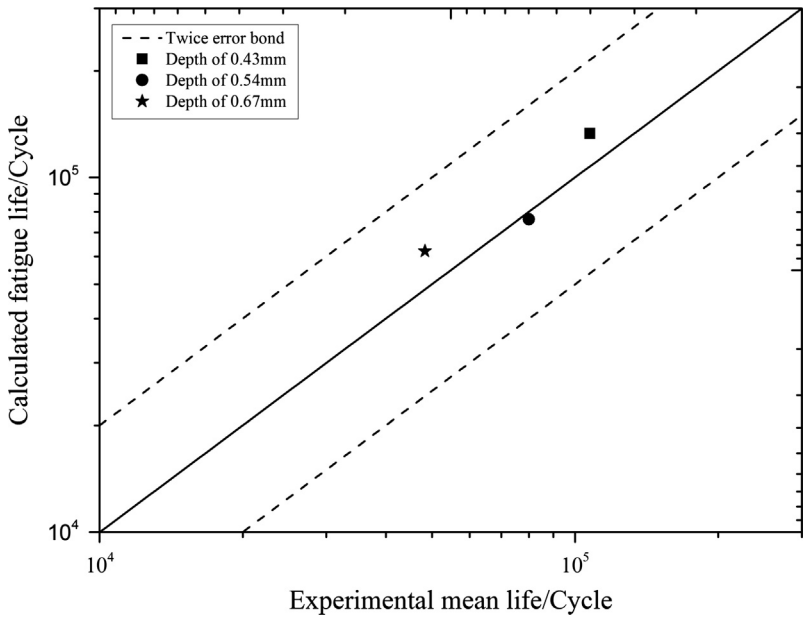

Fig. 10. Comparison between the calculated results and experimental data.

verification of stress convergence has been conducted to obtain an appropriate mesh size for the FEM simulation. The maximum values of longitudinal residual stress corresponding to the different mesh sizes are listed in Table 6. A minimum element size of 0.086 mm × 0.086 mm × 0.106 mm was finally adopted with the consideration of the computational accuracy and efficiency. In total, 54,372 elements and 50,800 nodes are created. The established finite element model is shown in Fig. 5.

In accordance with the experiment [8], the depth of impact is controlled to be 0.43 mm by exerting the corresponding displacement on the indenter. Subsequently, the residual stress and plastic strain fields can be obtained. The distribution of the longitudinal residual stress around the impact pit is shown in Fig. 6. The longitudinal residual stress along the depth direction away from the bottom of the impact pit is shown in Fig. 7. It is clear that the maximum longitudinal compressive stress is approximately 1.2 times the yield stress and is located 0.4 mm from the bottom of the impact pit. Then, the residual stress gradually decreases as the distance from the bottom of the impact pit increases and becomes a tensile stress at 1.2 mm from the bottom of the impact pit. Finally, the residual stress decreases to zero far away from the bottom of the impact pit. According to the plasticity damage model, the initial impact damage field around the impact pit can be calculated, with the distribution shown in Fig. 8. The initial impact damage is mainly focused on the surface layer of the impact pit, and the maximum initial damage is approximately 0.1.

4.3.2. Fatigue life calculation

Cyclic loading is applied in the longitudinal direction with a maximum applied stress of 500 MPa and a stress ratio of 0.1. The calculated fatigue life of the specimen considering the impact damage and residual stress relaxation effect is 133,150 cycles. The extent of the damage versus the number of cycles for the critical element is shown in Fig. 9. The fatigue damage accumulates from an initial damage value, which is induced by the impact. The elastic damage is relatively small, and the plastic damage plays a decisive

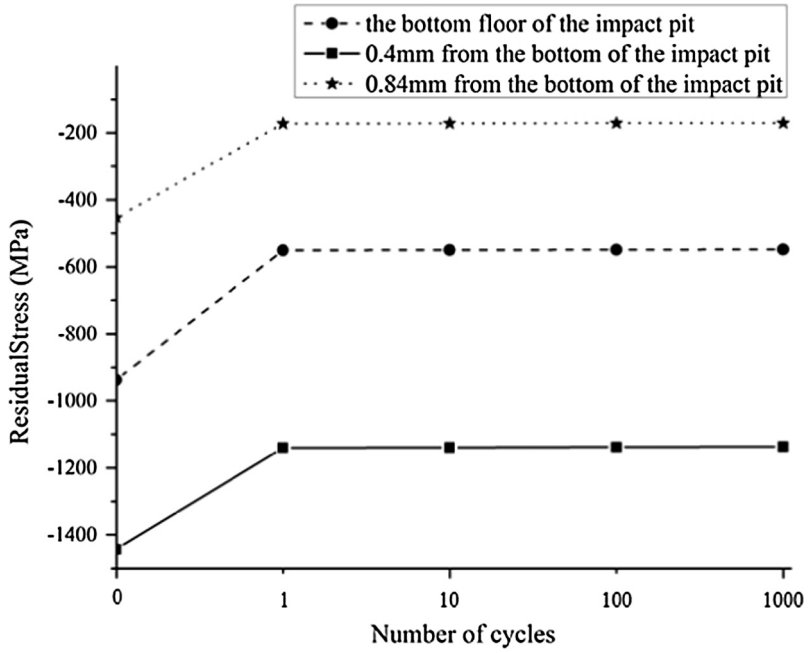

Fig. 11. The relaxation response of the longitudinal residual stress corresponding to the number of cycles.

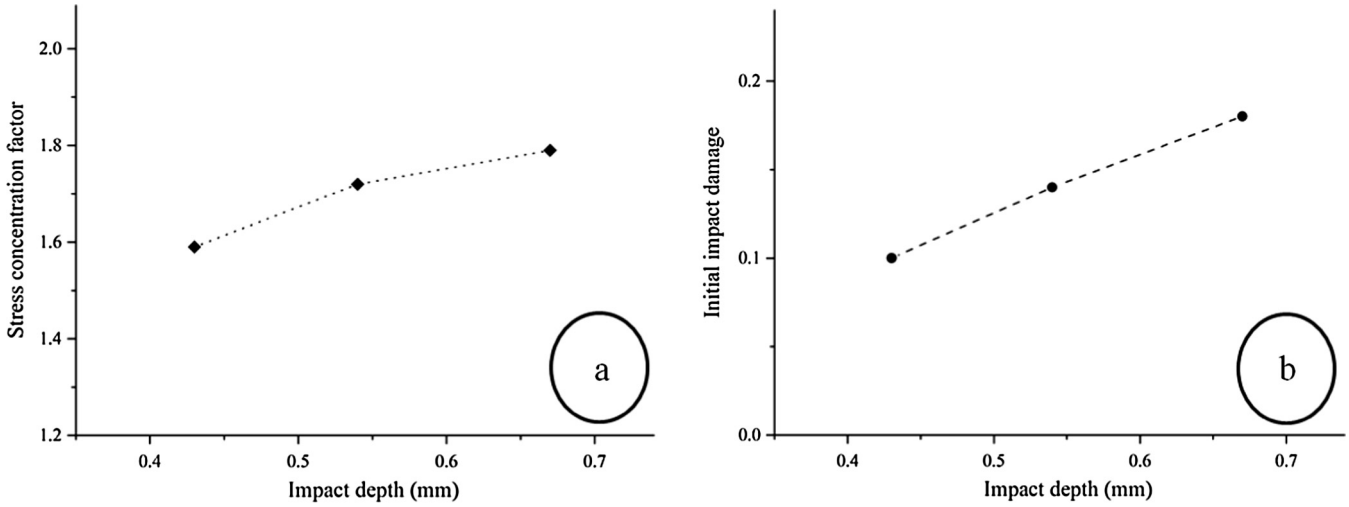

Fig. 12. Stress concentration factor and initial impact damage versus impact depth: (a) stress concentration factor and (b) initial impact damage.

role until the accumulation of damage at the critical element reaches 1, corresponding to fatigue crack initiation.

Based on the aforementioned computational method, the fatigue lives of specimens with different impact depths are also calculated. All of the experimental and calculated results are listed in Table 5. The calculated results are plotted versus the experimental mean life in Fig. 10. The experimental mean life is calculated according to the following formula: $N_{mean} = 10^{\wedge}\left(\frac{1}{n}\sum_{i=1}^{i=n}\lg N_{F_i}\right)$. Where N_{F_i} represents the experimental life of the ith specimen, n is the total number of specimens and N_{mean} represents the experimental mean life. It is clear that the calculated results agree well with the experimental data and all of the data are located within the twice error band.

4.3.3. Residual stress relaxation analysis

As we know, the residual stress induced by an impact can change the mean applied stress and stress ratio during the subsequent cyclic loading, which influences the fatigue life of the component. If the compressive residual stress around the impact pit shown in Fig. 6 is unchanged, this will likely greatly prolong the fatigue life. The residual stress field will vary when plastic deformation occurs around the impact pit during cyclic loading. Therefore, it is necessary to investigate changing the residual stress to evaluate the benefit of residual stress induced by impact. After the quasi-static simulation of impact process, the distribution of the residual stress around the impact pit can be obtained. Then the specimen with residual stresses was loaded by the cyclic loading. The stress field and damage field were calculated under each

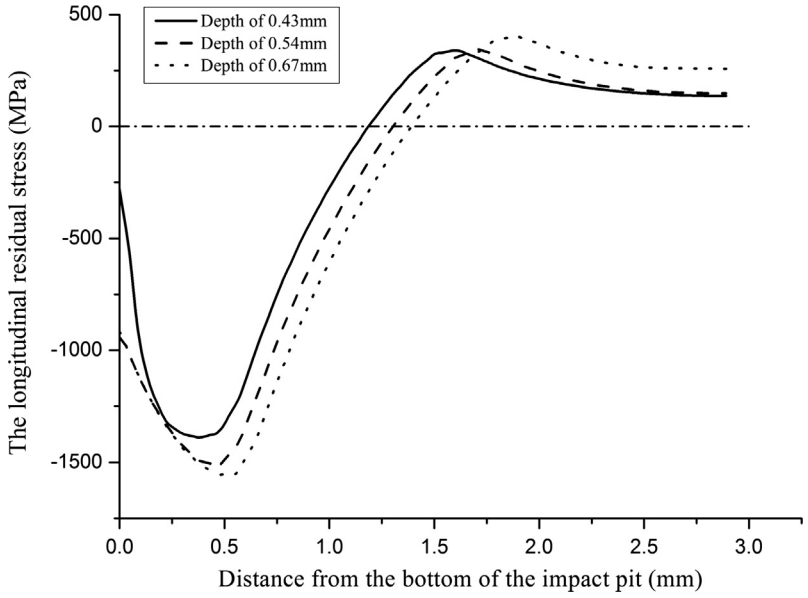

Fig. 13. The distribution of longitudinal residual stress with respect to the different impact depths.

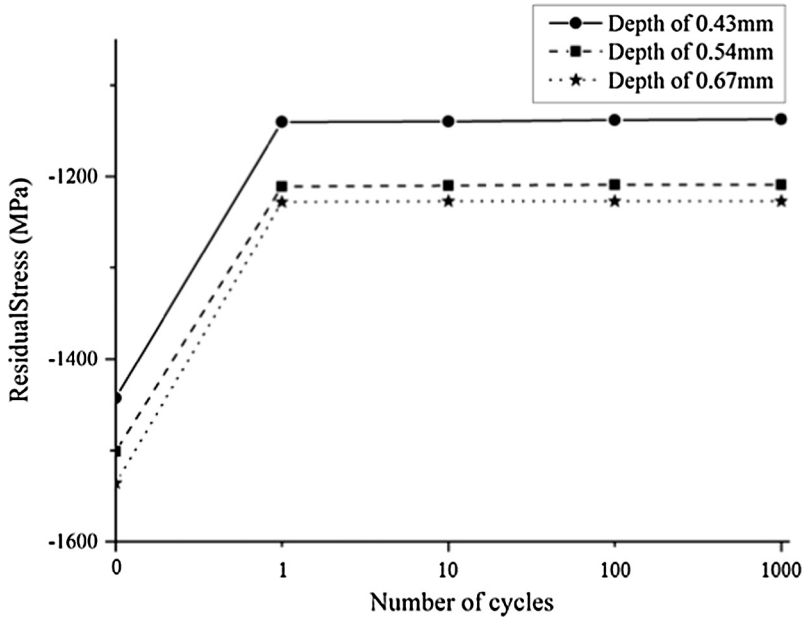

Fig. 14. The relaxation response of the longitudinal residual stress with respect to the different impact depths.

loading cycle, and the variation of the residual stress was then obtained. It should be noted that the result of residual stress relaxation was not calculated directly, but attributed to the damage of material causing the reduction of material stiffness. Fig. 11 shows the relaxation response for the longitudinal residual stress corresponding to the number of cycles. The different lines represent the different distances from the bottom of the impact pit. The relaxation of the residual stress mainly occurs in the first cycle. It is clear that the maximum reduction of residual compressive stress is approximately 60%. After the first cycle, there is almost no relaxation of the residual stress. This response of residual stress relaxation is consistent with the measured results of the experiment [23]. Additionally, one may also notice that the residual stress is still compressive, despite the occurrence of relaxation. Thus, the benefit from residual stress is consistent during the entire process of cyclic loading.

5. Discussions

In this section, the influencing factors of impact depth and radius of impact object are discussed respectively. Three aspects of the effects of the influencing factors are presented in detail: (1) effects on the local stress concentration, initial impact damage and residual stress distribution; (2) effects on the residual stress relaxation and elastic-plastic damage evolution; and (3) effects on the fatigue life.

5.1. Effects of the impact depth

The impact depths discussed in this section are 0.43 mm, 0.54 mm and 0.67 mm, respectively. The radius of the impact object is 1.0 mm for all three cases.

5.1.1. Effects on the local stress concentration, initial impact damage and residual stress distribution

The impact depth has direct effects on the local stress concentration, initial impact damage and residual stress distribution. For depths of 0.43 mm, 0.54 mm and 0.67 mm, the corresponding stress concentration factors are 1.59, 1.72 and 1.79, respectively. The differences among these values are insignificant. After the quasi-static simulation of the impact process, the initial impact damages are calculated, which are 0.093, 0.128 and 0.167, respectively. The

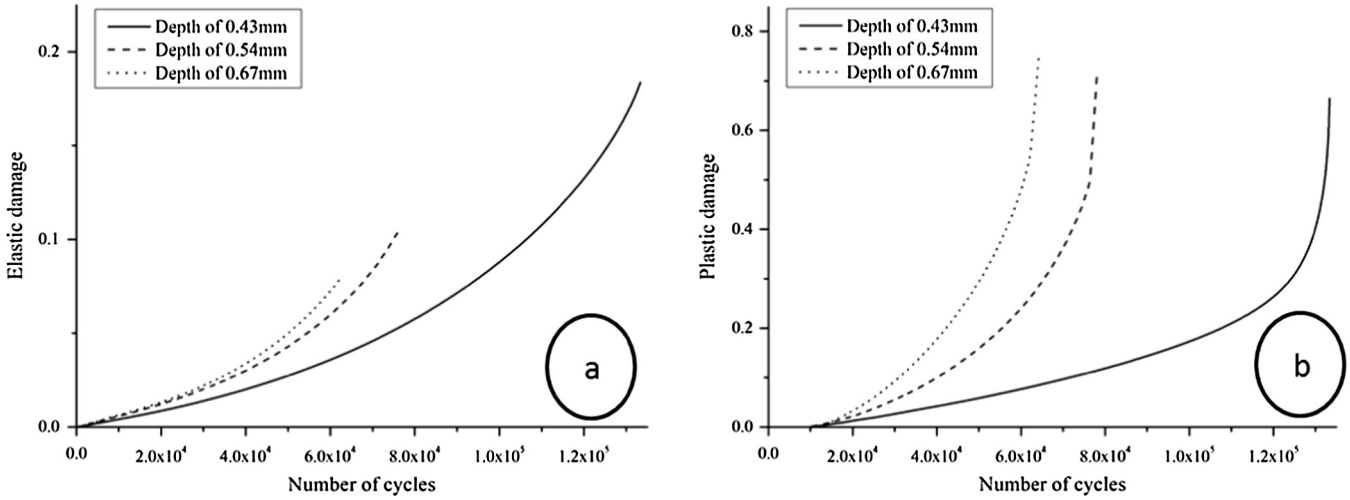

Fig. 15. Damage versus the number of cycles with respect to different impact depths: (a) elastic damage and (b) plastic damage.

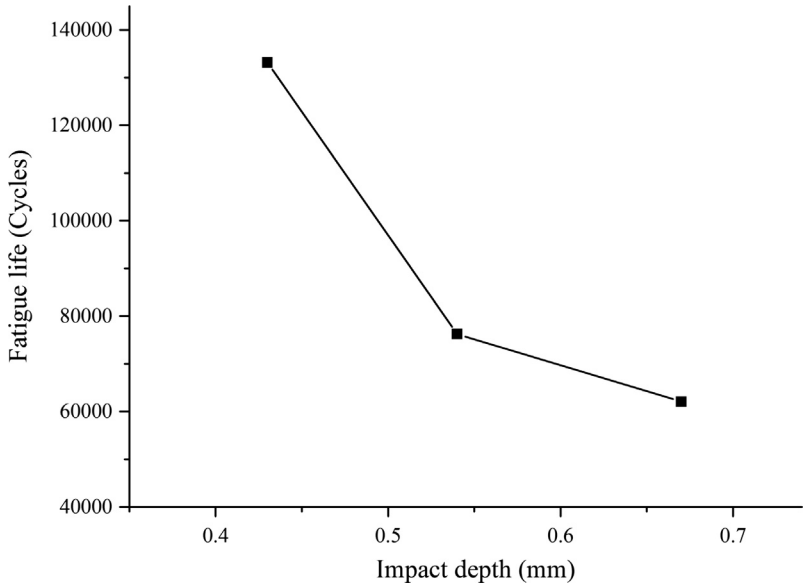

Fig. 16. Fatigue life versus impact depth.

relationships between the stress concentration factors and initial impact damages versus the impact depth are shown in Fig. 12. It is clear that the deeper the impact depth, the larger the initial impact damage and the more severe the stress concentration caused by the impact. Thus, from this point of view, the fatigue life of the specimen will decrease as the impact depth increases.

The distributions of the longitudinal residual stress along the distance from the bottom of the impact pit with respect to the different depths of impact are shown in Fig. 13. The changing trends for residual stress are similar, and the maximum longitudinal residual stress slightly increases with the impact depth. The longitudinal compressive residual stress close to the surface is desirable when trying to increase fatigue life.

5.1.2. Effects on the residual stress relaxation and elastic-plastic damage evolution

When the specimen undergoes fatigue loading at a relatively high stress, inelastic strain occurs. Correspondingly, elastic-plastic damage is induced as a change in the residual stress state observed. The relaxation response of the maximum longitudinal residual stress with respect to the different depths of the impact pits are shown in Fig. 14 for specimens with impact pits of different depths that are subjected to the same far field stress. For all cases, the relaxation responses of the maximum longitudinal residual stress mainly occur in the first cycle, and the magnitudes of the decrease in the residual stress are almost the same, even when the maximum values of the residual stress are different.

The elastic and plastic damage in the critical element versus the number of cycles are shown in Fig. 15. The increasing trend of the elastic-damage damage is similar and increases slowly in the beginning before accelerating. The subsequent plastic damage then starts to dominate compared to the elastic damage. The damage evolution rate increases with the depth of the impact pits, which is mainly attributed to the increase in the stress concentration. The differences among the three cases examined here are insignificant, whereas the fatigue life is sensitive to the stress level.

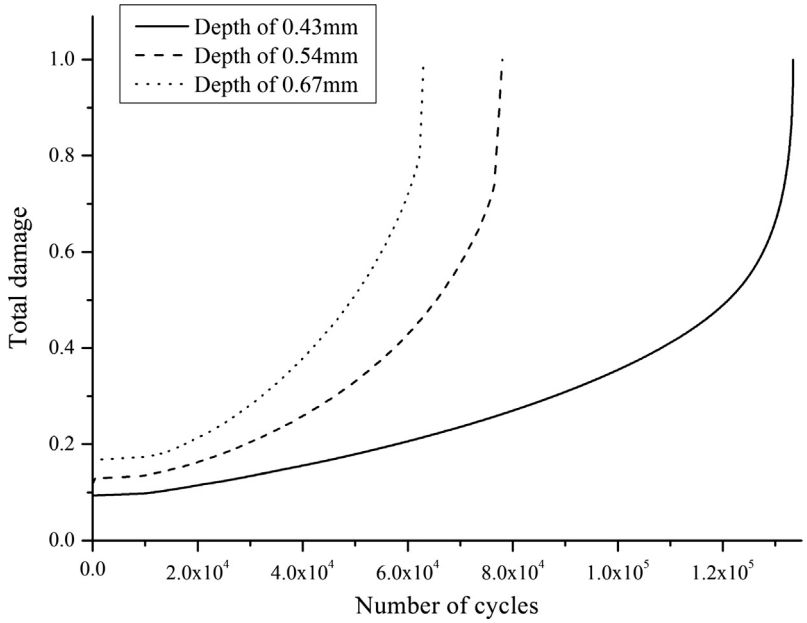

Fig. 17. Total damage versus the number of cycles for different impact depths.

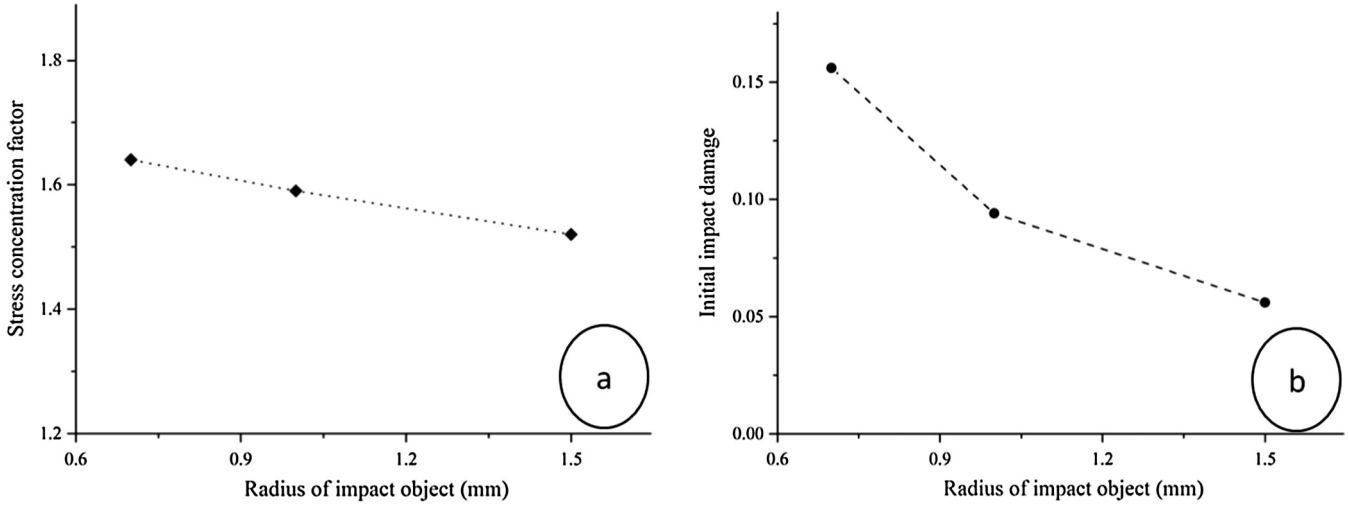

Fig. 18. Stress concentration factors and initial impact damage versus impact radius: (a) stress concentration factor and (b) initial impact damage.

5.1.3. Effects on the fatigue life

The fatigue lives of specimens with different impact depths were calculated. The fatigue life versus impact depth is plotted in Fig. 16, and the relationship between the total damage versus the number of cycles corresponding to the dangerous element is plotted in Fig. 17. The fatigue life decreases with the increase in the impact depth. In conclusion, the fatigue life depends on the competitive mechanisms of the initial impact damage, local stress concentration, and compressive residual stress. The longitudinal compressive residual stress close to the surface can benefit the fatigue life. However, the initial impact damage and local stress concentrations have negative effects on the fatigue life.

5.2. Effects of the radius of the impact object

The radius of the impact object is another important factor influencing elastic-plastic damage and fatigue life. The radii of the impact objects discussed in this section are 0.7 mm, 1.0 mm and 1.5 mm, respectively. The depth of impact is 0.43 mm.

5.2.1. Effects on the local stress concentration, initial impact damage and residual stress distribution

For radii of 0.7 mm, 1.0 mm and 1.5 mm, the corresponding stress concentration factors are 1.64, 1.59 and 1.52, respectively, which are slightly different from each other. The corresponding initial impact damages are 0.156, 0.094 and 0.056, respectively. The stress concentration factors and initial impact damages versus the radius of the impact object are plotted in Fig. 18. The smaller the radius, the larger the initial impact damage and the more severe the stress concentration caused by the impact. This leads to a decrease in fatigue life as the radii of impact object decreases.

The distributions of the longitudinal residual stress along the distance from the bottom of the impact pit with respect to the radius of the impact object are shown in Fig. 19. The absolute value

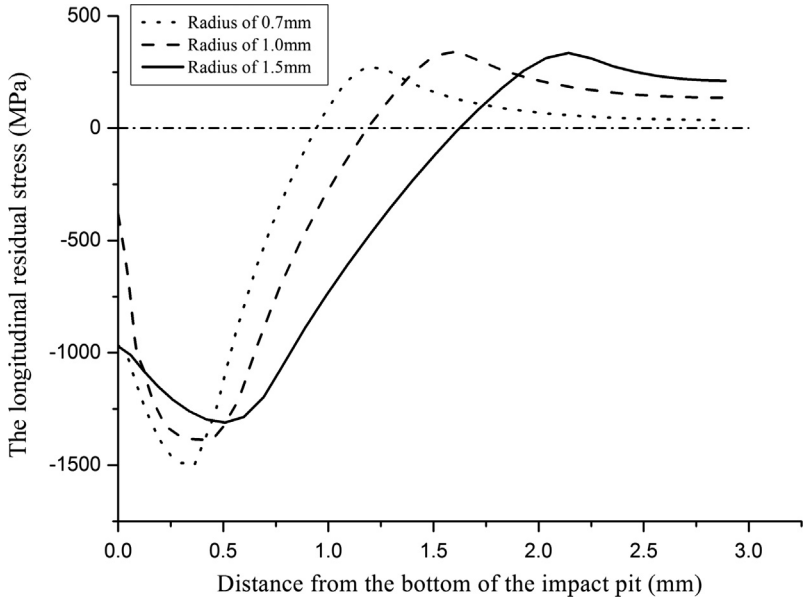

Fig. 19. The distribution of the longitudinal residual stress with respect to the radius of the impact object.

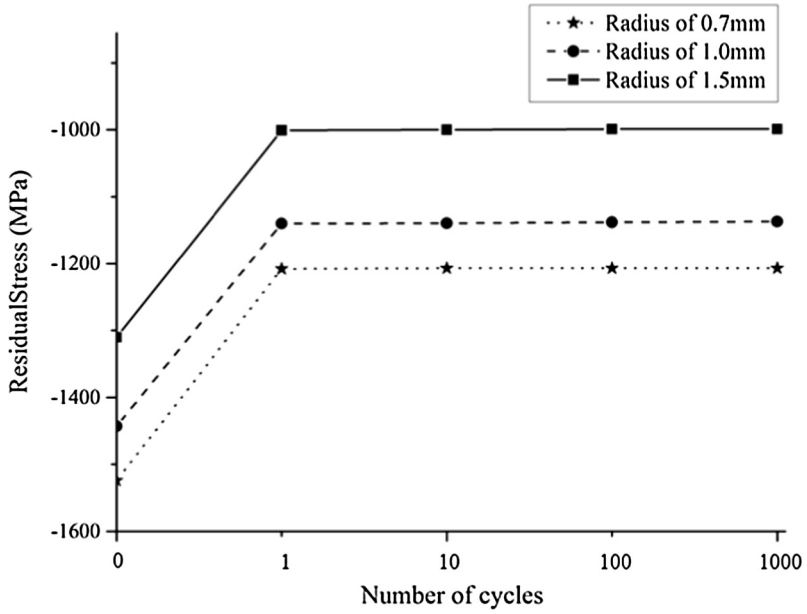

Fig. 20. The relaxation response of the longitudinal residual stress with respect to the radius of the impact object.

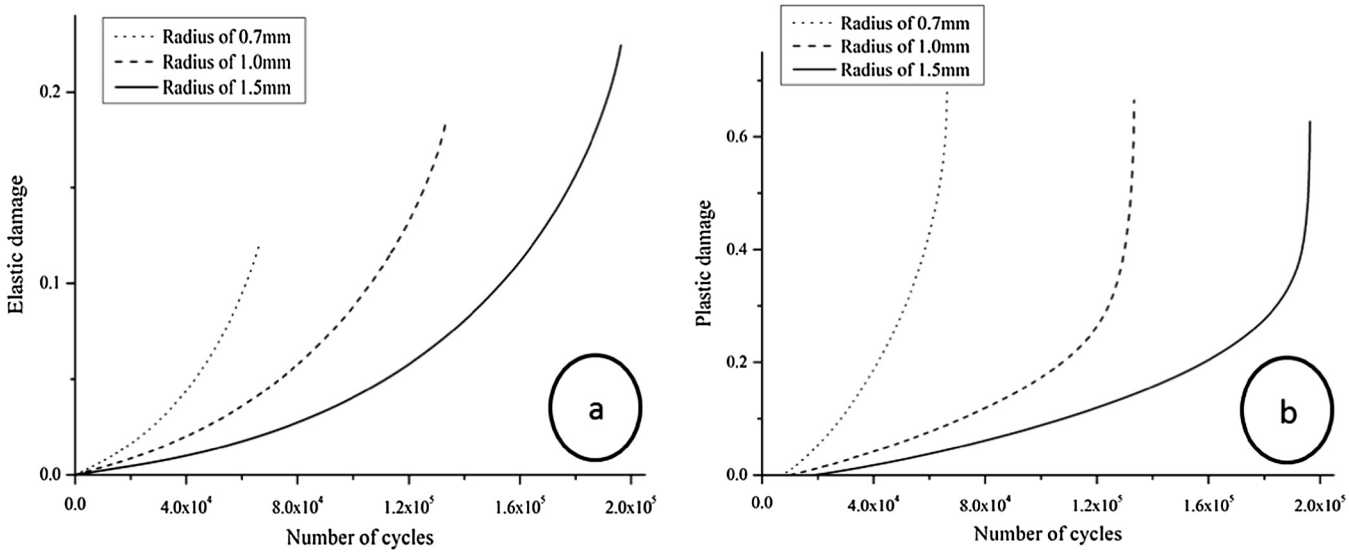

Fig. 21. Damage versus the number of cycles with respective to the different impact radii: (a) elastic damage and (b) plastic damage.

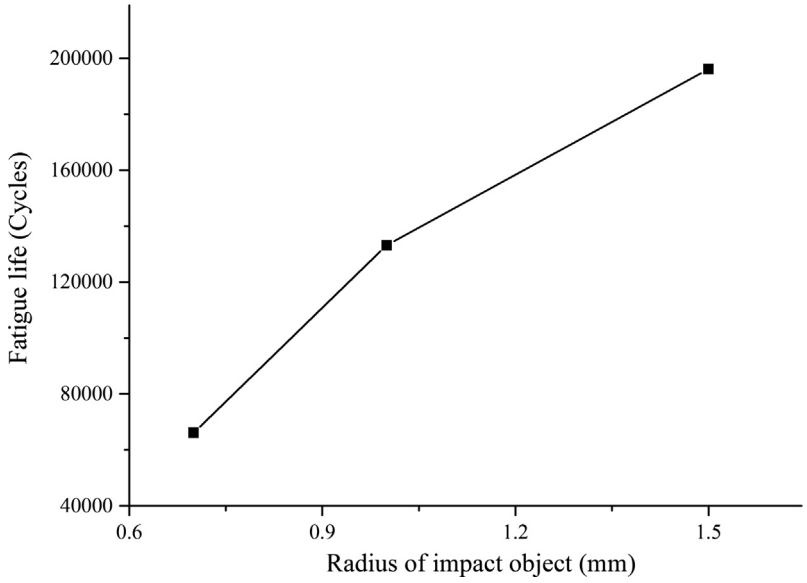

Fig. 22. Fatigue life versus radius of the impact object.

of the maximum longitudinal residual stress increases slightly as the radius of the impact object decreases, whereas the range of the compressive residual stress becomes wider when the radius of the impact object is bigger.

5.2.2. Effects on the residual stress relaxation and elastic-plastic damage evolution

The relaxation response of the maximum longitudinal residual stress corresponding to the number of cycles is shown in Fig. 20. It is clear that the relaxation responses mainly occur in the first cycle. The compressive residual stress increases as the radius of the impact object decreases, whereas the magnitudes of the reductions are almost the same for the three cases.

Relationships between the elastic and plastic damage of the critical element versus number of cycles are shown in Fig. 21. The final elastic damage increases with the radius and the final plastic damage decreases as the radius increases. For all of the impact radii, plastic damage dominates in the final total damage compared with elastic damage.

5.2.3. Effects on the fatigue life

For impact radii of 0.7 mm, 1.0 mm and 1.5 mm, the calculated fatigue lives are 66,150, 133,150 and 196,150 cycles, respectively. The fatigue life versus the radius of the impact object is shown in Fig. 22, and the total damage versus the number of cycles of the critical element are shown in Fig. 23. The fatigue life decreases with the impact radius. The fatigue life depends on the competitive mechanisms behind the initial impact damage, local stress concentration and the compressive residual stress.

6. Conclusions

In this study, a new approach to fatigue life calculation that considers impact damage, residual stress relaxation and elastic-plastic fatigue damage is proposed based on the continuum damage mechanics theory. The following conclusions can be made:

(1) A quasi-static simulation analysis of the impact process is conducted, and the residual stress and plastic strain fields

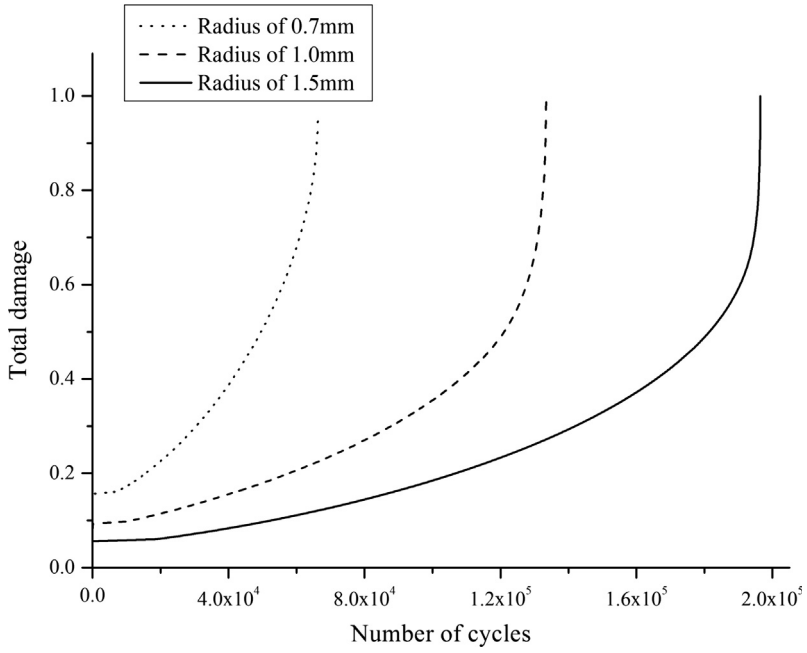

Fig. 23. Total damage versus the number of cycles for different impact radii.

are obtained. Then, the initial impact damage around the impact pit is calculated according to Lemaitre's ductile damage model.

(2) The damage-coupled elastic-plastic constitutive equations and fatigue damage evolution equations are derived to calculate the stress and strain in the material, the degradation of the material and the elastic-plastic damage to the material during cyclic loading.

(3) The finite element implementation corresponding to the theoretical models is presented, and the fatigue life is calculated taking into account the coupling effect of the stress field, residual stress relaxation and damage field. The calculated results are in accordance with the experimental data available in the literature.

(4) Two factors influencing the elastic-plastic damage and fatigue life are discussed. The increase in the impact depth and decrease in the radius of the impact object both lead to decreases in fatigue life, but have little influence on the residual stress relaxation trend. The residual stress relaxation mainly occurs during the first cycle of loading. After approximately 1000 cycles, there is almost no relaxation of the residual stress.

References

[1] Giglio M, Beretta S, Mariani U, et al. Defect tolerance assessment of a helicopter component subjected to multiaxial load. Eng Fract Mech 2010;77(13):2479–90.
[2] Lazzeri L, Mariani U. Application of damage tolerance principles to the design of helicopters. Int J Fatigue 2009;31(6):1039–45.
[3] Zhan Z, Hu W, Zhang M, et al. Experimental method for and theoretical research on defect tolerance of fixed plate based on damage mechanics. Chin J Aeronaut 2013;26(5):1195–201.
[4] Socie DF. Fatigue-life prediction using local stress-strain concepts. Exp Mech 1977;17(2):50–6.
[5] Gough HJ, Pollard HV. The strength of metals under combined alternating stresses. Proc Inst Mech Eng 1935;131(1):3–103.
[6] Marandi SM, Rahmani K, Tajdari M. Foreign object damage on the leading edge of gas turbine blades. Aerosp Sci Technol 2014;33(1):65–75.
[7] Ruschau JJ, Nicholas T, Thompson SR. Influence of foreign object damage (FOD) on the fatigue life of simulated Ti-6Al-4V airfoils. Int J Impact Eng 2001;25(3):233–50.
[8] Peters JO, Ritchie RO. Influence of foreign-object damage on crack initiation and early crack growth during high-cycle fatigue of Ti–6Al–4V. Eng Fract Mech 2000;67(3):193–207.
[9] Chaboche JL. Continuous damage mechanics—a tool to describe phenomena before crack initiation. Nucl Eng Des 1981;64(2):233–47.
[10] Kachanov L. Introduction to continuum damage mechanics. Springer; 1986. p. 1–10.
[11] Lemaitre J. A course on damage mechanics. Berlin: Springer; 1996. p. 1–10.
[12] Zhan Z, Hu W, Meng Q, et al. Continuum damage mechanics-based approach to the fatigue life prediction for 7050–T7451 aluminum alloy with impact pit. Int J Damage Mech 2016;25(7):943–66.
[13] Webster GA, Ezeilo AN. Residual stress distributions and their influence on fatigue lifetimes. Int J Fatigue 2001;23:375–83.
[14] Torres MAS, Voorwald HJC. An evaluation of shot peening, residual stress and stress relaxation on the fatigue life of AISI 4340 steel. Int J Fatigue 2002;24(8):877–86.
[15] Schijve J. Fatigue of structures and materials. Dordrecht: Kluwer Academic; 2001.
[16] Wang JS, Hsieh CC, Lin CM, et al. The effect of residual stress relaxation by the vibratory stress relief technique on the textures of grains in AA 6061 aluminum alloy. Mater Sci Eng, A 2014;605:98–107.
[17] Laamouri A, Sidhom H, Braham C. Evaluation of residual stress relaxation and its effect on fatigue strength of AISI 316L stainless steel ground surfaces: experimental and numerical approaches. Int J Fatigue 2013;48:109–21.
[18] Madariaga A, Esnaola JA, Arrazola PJ, et al. Stability of machining induced residual stresses in Inconel 718 under quasi-static loading at room temperature. Mater Sci Eng, A 2015;620:129–39.
[19] Kim JC, Cheong SK, Noguchi H. Residual stress relaxation and low-and high-cycle fatigue behavior of shot-peened medium-carbon steel. Int J Fatigue 2013;56:114–22.
[20] Juijerm P, Altenberger I, Scholtes B. Fatigue and residual stress relaxation of deep rolled differently aged aluminum alloy AA6110. Mater Sci Eng, A 2006;426(1):4–10.
[21] Zaroog OS, Ali A, Sahari BB, et al. Modeling of residual stress relaxation of fatigue in 2024–T351 aluminum alloy. Int J Fatigue 2011;33(2):279–85.
[22] Madariaga A, Esnaola JA, Arrazola PJ, et al. Stability of machining induced residual stresses in Inconel 718 under quasi-static loading at room temperature. Mater Sci Eng, A 2015;620:129–39.
[23] Boyce BL, Chen X, Peters JO, et al. Mechanical relaxation of localized residual stresses associated with foreign object damage. Mater Sci Eng, A 2003;349(1):48–58.
[24] Zhuang WZ, Halford GR. Investigation of residual stress relaxation under cyclic load. Int J Fatigue 2001;23:31–7.
[25] Mattson RL, Coleman WS. Effect of shot-peening variables and residual stresses on the fatigue life of leaf-spring specimens. Trans, Soc Automot Eng 1954;62:546–56.
[26] Frija M, Hassine T, Fathallah R, et al. Finite element modelling of shot peening process: prediction of the compressive residual stresses, the plastic deformations and the surface integrity. Mater Sci Eng, A 2006;426(1):173–80.
[27] Boyce BL, Chen X, Hutchinson JW, et al. The residual stress state due to a spherical hard-body impact. Mech Mater 2001;33(8):441–54.

[28] Lemaitre J, Chaboche JL. Mechanics of solid materials. Cambridge: Cambridge University Press; 1990.
[29] Lemaitre J. Mechanics of solid materials. Cambridge University Press; 1994. p. 346–449.
[30] Lemaitre J, Desmorat R. Engineering damage mechanics: ductile, creep, fatigue and brittle failures. Springer; 2005. p. 188–9.
[31] Chaboche JL. On some modifications of kinematic hardening to improve the description of ratchetting effects. Int J Plast 1991;7(7):661–78.
[32] Kang G, Liu Y, Ding J, et al. Uniaxial ratcheting and fatigue failure of tempered 42CrMo steel: damage evolution and damage-coupled visco-plastic constitutive model. Int J Plast 2009;25(5):838–60.
[33] Chaboche JL, Lesne PM. A non-linear continuous fatigue damage model. Fatigue Fract Eng Mater Struct 1988;11(1):1–17.
[34] Marmi AK, Habraken AM, Duchene L. Multiaxial fatigue damage modelling at macro scale of Ti–6Al–4V alloy. Int J Fatigue 2009;31(11):2031–40.
[35] Zhan Z, Hu W, Zhang M, et al. The fatigue life prediction for structure with surface scratch considering cutting residual stress, initial plasticity damage and fatigue damage. Int J Fatigue 2015;74:173–82.
[36] Shen F, Hu W, Meng Q. A non-local approach based on the hypothesis of damage dissipation potential equivalence to the effect of stress gradient in fretting fatigue. Int J Fatigue 2016;90:125–38.
[37] Shen F, Hu W, Voyiadjis GZ, et al. Effects of fatigue damage and wear on fretting fatigue under partial slip condition. Wear 2015;338:394–405.
[38] Military Handbook – MIL-HDBK-5H: metallic materials and elements for aerospace vehicle structures.US Department of Defense; 1998.
[39] Wu XR. Handbook of mechanical properties of aircraft structural metals, vol. 1. Beijing: Aviation Industry Press; 1998.